Supporting Information

Novel Cu(Zn)-Ge-P compounds as advanced anode materials for Li-ion batteries

Wenwu Li,*[a,b] Pengfei Shen,[b] Lufeng Yang,[c] Anjie Chen,[d] Jeng-Han Wang,[d] Yunyong Li[b], Hailong Chen,[c] and Meilin Liu*[a]

a. School of Materials Science & Engineering, Georgia Institute of Technology, Atlanta, GA, 30332, USA

b. School of Materials and Energy, Guangdong University of Technology, Guangzhou 510006, PR China.

c. The Woodruff school of Mechanical Engineering, Georgia Institute of Technology, 771 Ferst Drive, Atlanta, GA, 30332, USA

d. Department of Chemistry, National Taiwan Normal University, Taipei, 11677, Taiwan.

Table S1. Key processing and refinement parameters of $CuGe_2P_3$ sample.

Compound	$CuGe_2P_3$
Crystal System	Cubic
Space Group	F-43m
Point Group	CF6
a Å	5.354425
V $Å^3$	153.511
2θ-interval º	5-130
Z	1
Rwp%	1.64
Rp%	1.28
^{2}	1.594

Table S2. Fractional atomic coordinates and isotropic displacement parameters ($Å^2$) of $CuGe_2P_3$.

	x	y	z	U_{iso}	Occ
Cu	0	0	0	0.25128	0.333
Ge	0	0	0	0.25128	0.667
P	0.25	0.25	0.25	0.00689	1

Table S3. Synchrotron radiation angle information of the $CuGe_2P_3$.

	$CuGe_2P_3$ Powder								
2θ	4.435°	5.03°	7.258°	7.616°	8.506°	10.266°	11.187°	12.576°	13.344°
Relative intensity	100	10.46	54.3	6.97	29.17	8.07	11.82	12.25	7.24

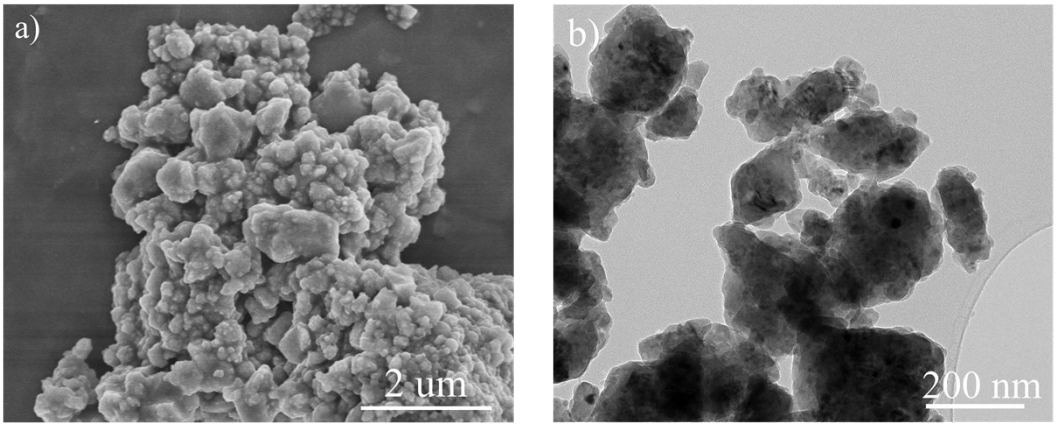

Fig. S1. Morphology characterizations of $CuGe_2P_3$ compound at low magnification: a) The FESEM image; b) the TEM image.

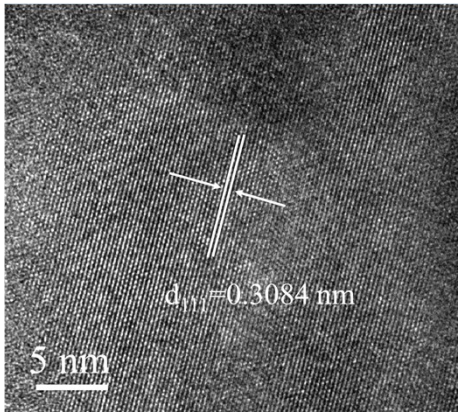

Fig. S2. HRTEM image of as-synthesized cubic $CuGe_2P_3$.

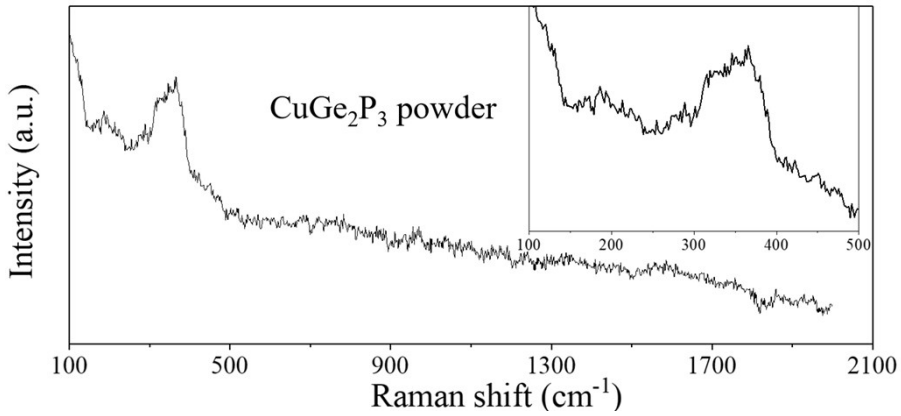

Fig. S3. Raman spectroscopy of the cation-disordered $CuGe_2P_3$ compound.

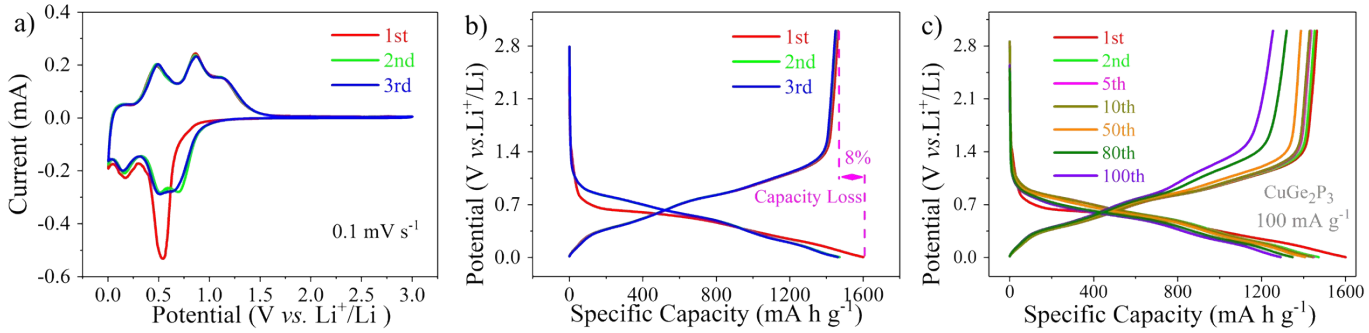

Fig. S4. a) Initial three CV curves and b) initial three discharge-charge profiles of the cation-disordered $CuGe_2P_3$ compound; c) voltage profiles of different cycling conditions of $CuGe_2P_3$ compound at 100 mA h g^{-1}.

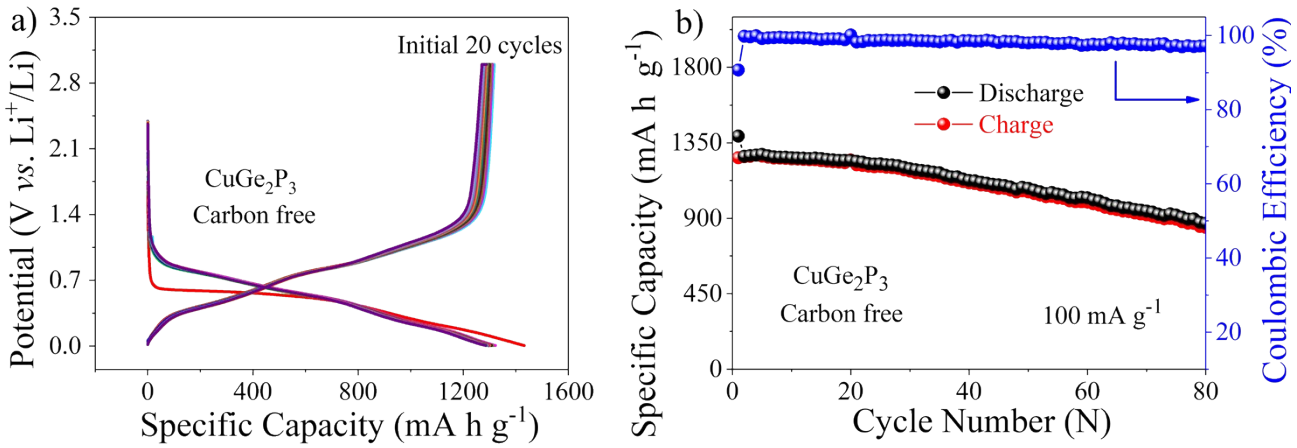

Fig. S5. Typical discharge-charge curves and cycle performance of the cation-disordered $CuGe_2P_3$ compound without any conductive agents.

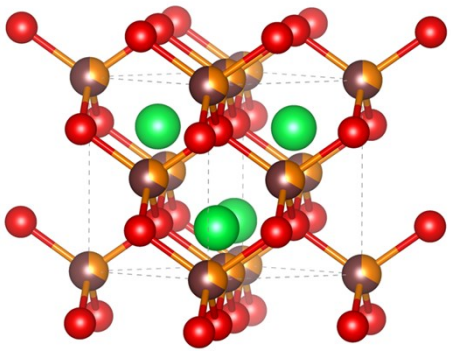

Fig. S6. The crystal structure of $Li_3CuGe_2P_3$, which derived from the Li-insertion voids within the crystal structure of the cation-disordered $CuGe_2P_3$ compound.

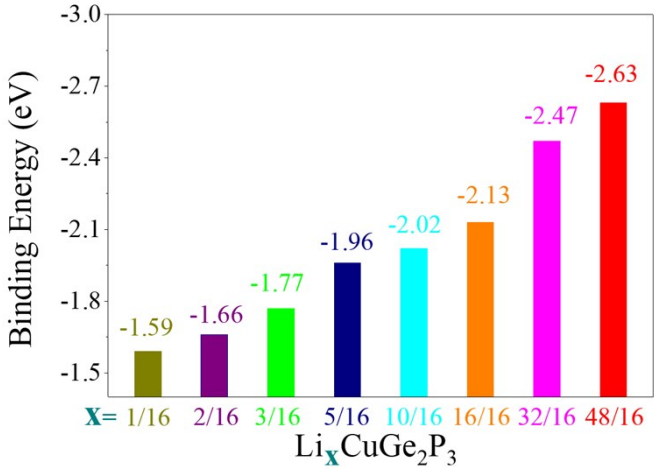

Fig. S7. Binding energies of cation-disordered $CuGe_2P_3$ with various Li atom number inserted in the voids by first-principles calculations.

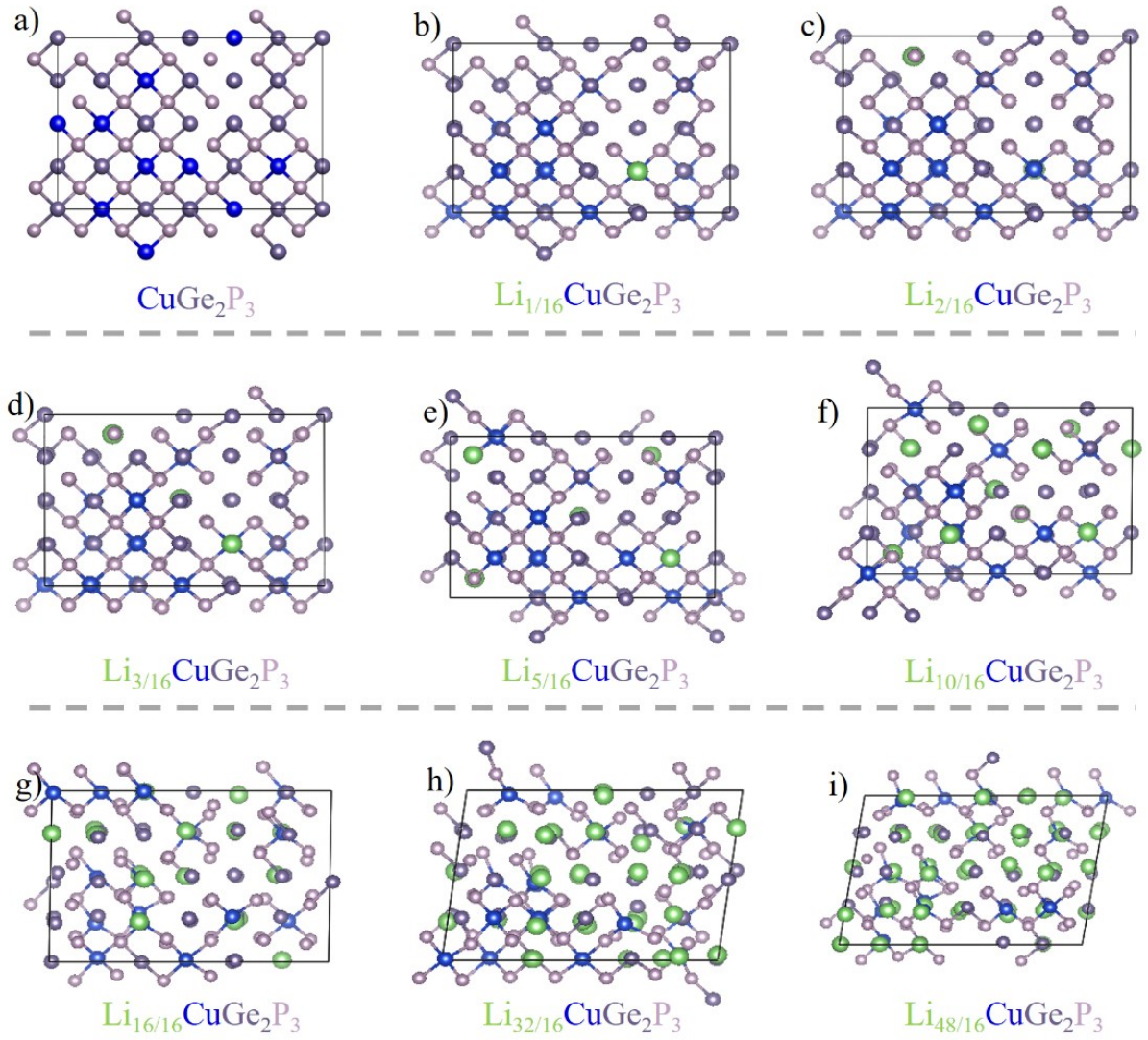

Fig. S8. The corresponding supercell models in Fig. S7.

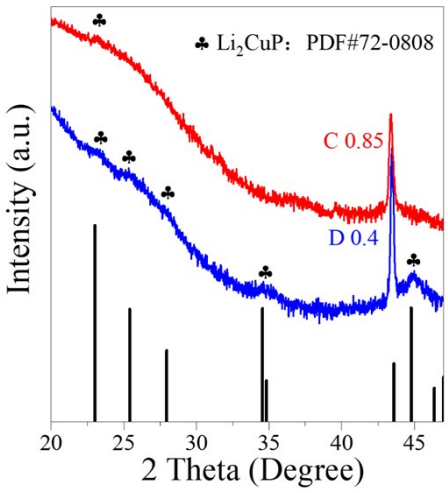

Fig. S9. The enlarged XRD patterns at the state of discharging to 0.4 V and charging to 0.85 V.

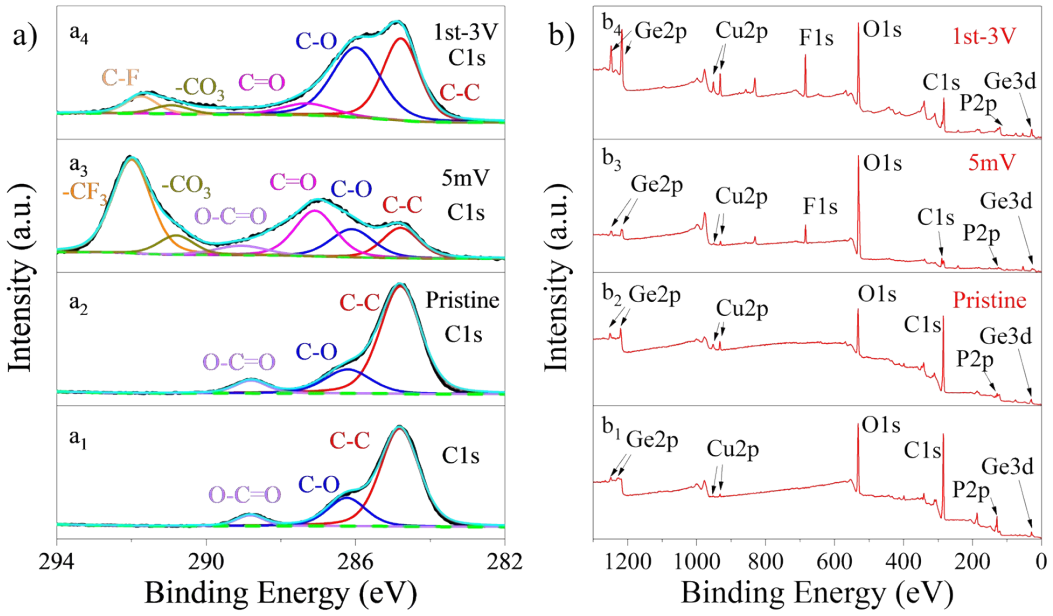

Fig. S10. High-resolution XPS spectra of the cation-disordered $CuGe_2P_3$ compound electrodes after initial cycling, the discharge state of 5 mV, pristine $CuGe_2P_3$ sample and raw materials of Ge, P and Cu.

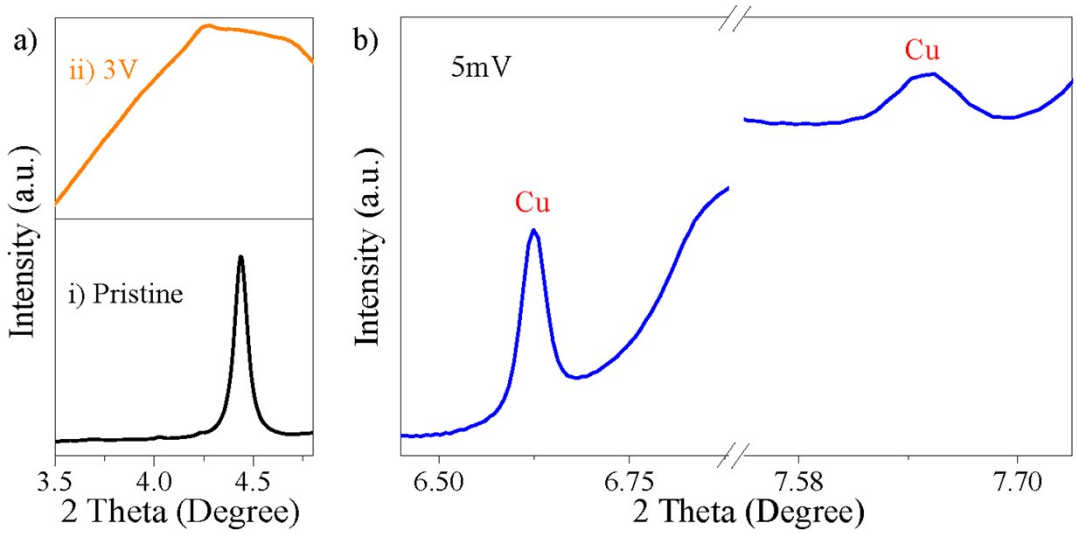

Fig. S11. The ex-situ high-resolution synchrotron X-ray diffraction patterns of $CuGe_2P_3$ anodes at different potentials.

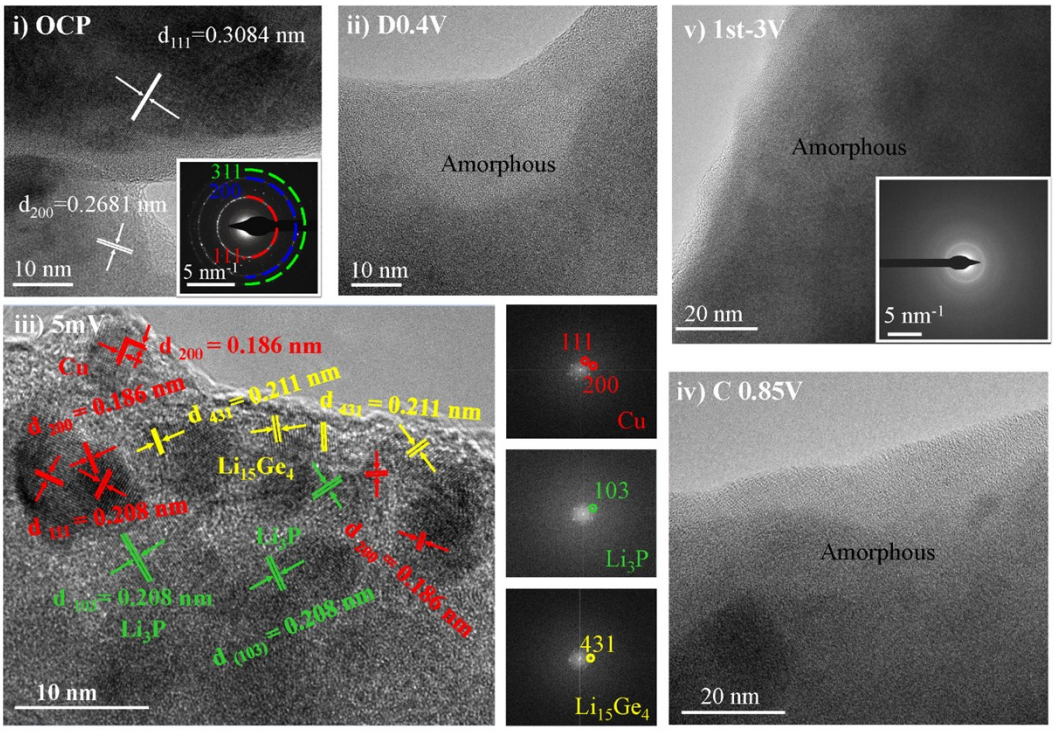

Fig. S12. Ex-situ HRTEM images of the cation-disordered $CuGe_2P_3$ compound anodes at different potentials.

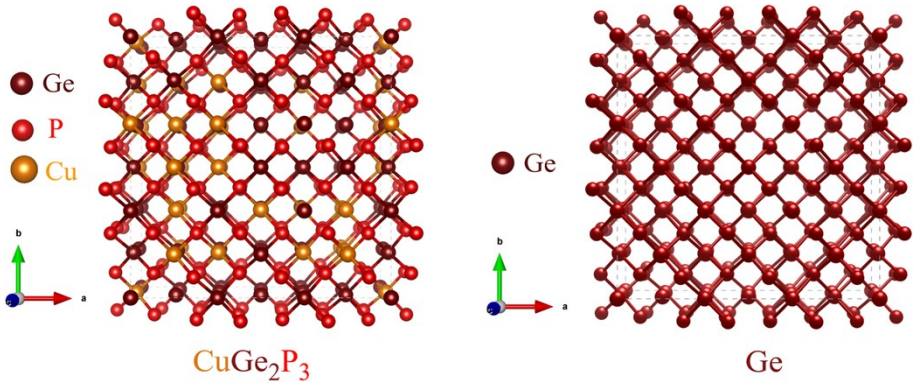

Fig. S13. Simulation models utilized for first-principles calculations of the cation-disordered $CuGe_2P_3$ and Ge.

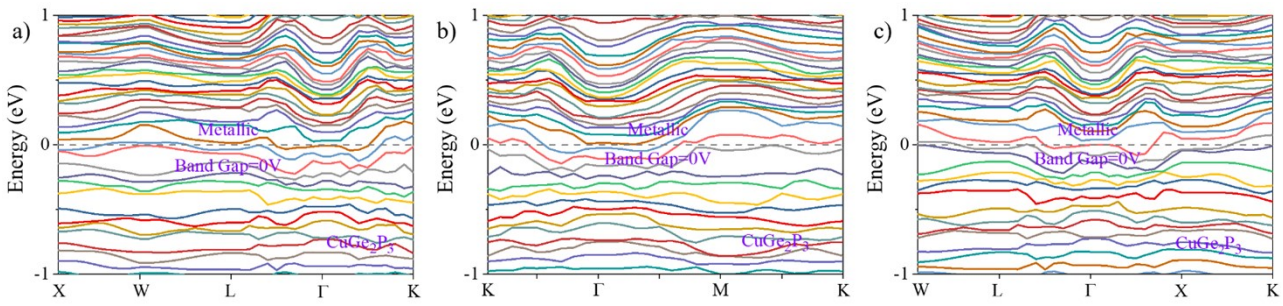

Fig. S14. Band structures of the cation-disordered $CuGe_2P_3$.

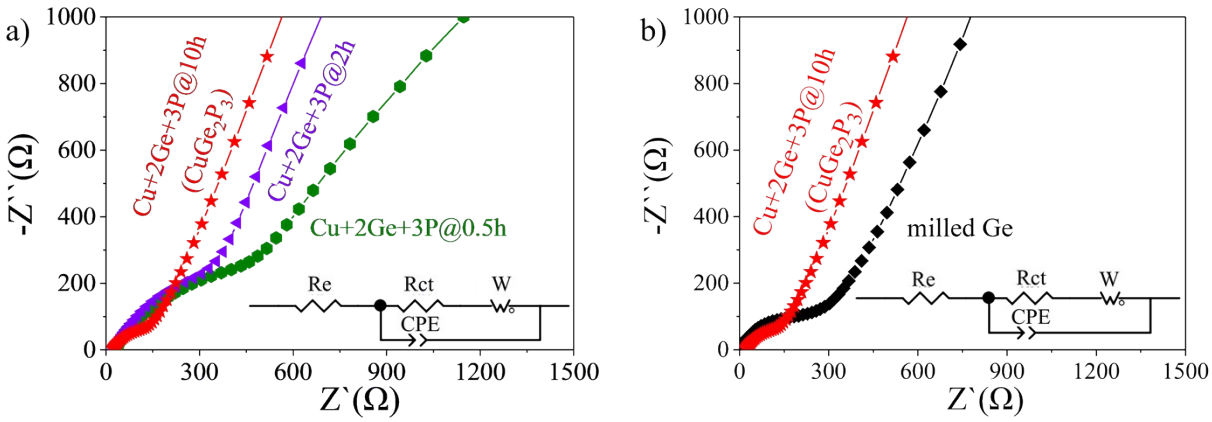

Fig. S15. Electrochemical impedance spectroscopy of the cell with a) ball milled Cu+2Ge+3P samples and, b) ball milled Ge powder.

Table S4. The tested electronic conductivity of the $CuGe_2P_3$-based electrode ($CuGe_2P_3$: carbon black: binder = 7: 2: 1), $CuGe_2P_3$ powder, Ge powder, the mixed Cu+2Ge+3P powder and red P powder under the mild pressure and room temperature.

Materials	Conductivity (S m^{-1})
$CuGe_2P_3$ electrode	331
$CuGe_2P_3$	68
Ge	0.089
mixed Cu+2Ge+3P	0.03
red P	less than 10^{-5}

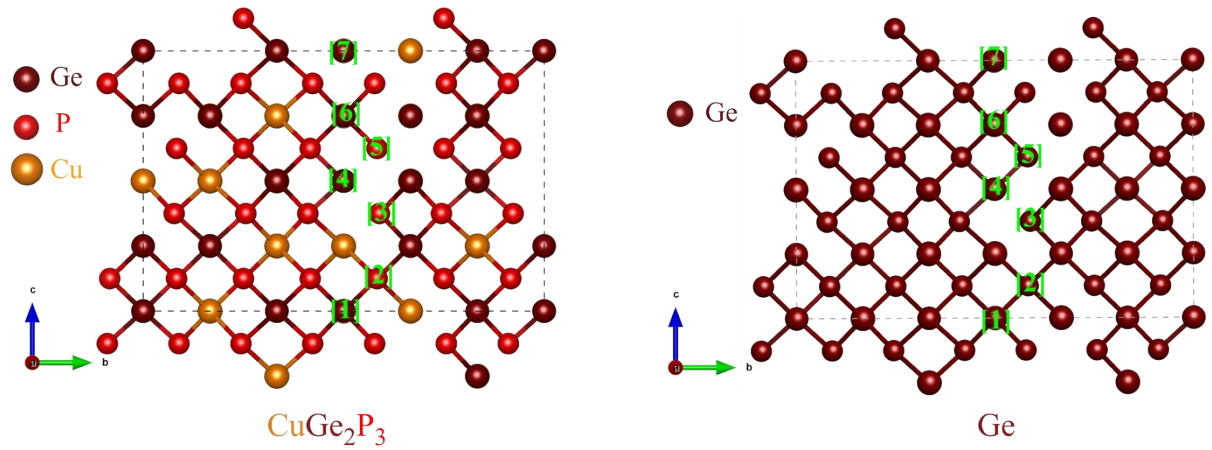

Fig. S16. Typical Li-ion migration paths of the cation-disordered $CuGe_2P_3$ and Ge.

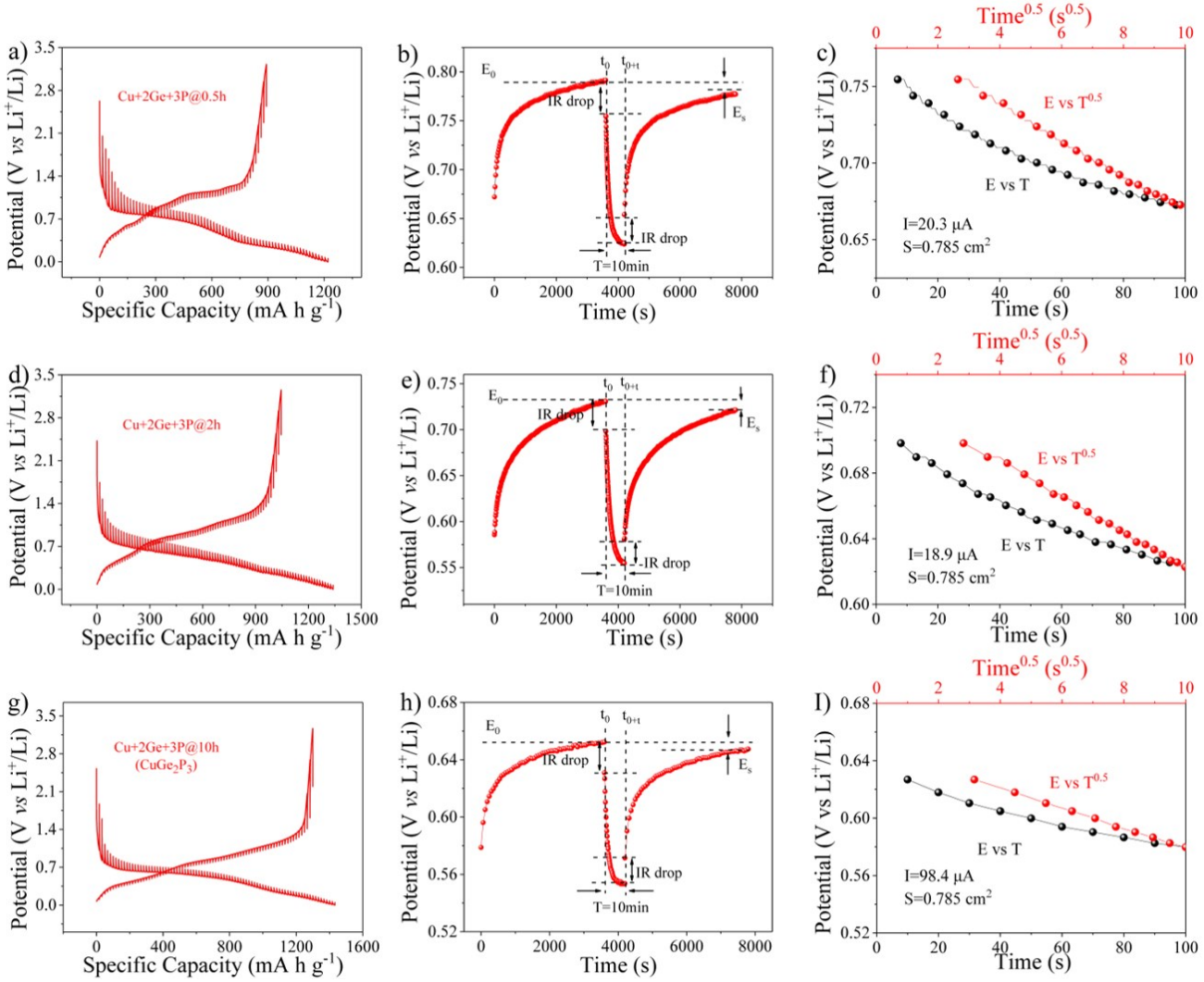

Fig. S17. a), d) and g) Galvanostatic intermittent titration technique (GITT) profiles during first-cycle discharge-charge of LIBs utilizing the ball milled Cu+2Ge+3P samples; b), e) and h) typical schemes for single-step of GITT experiments of LIBs utilizing the ball milled Cu+2Ge+3P samples; c), f) and I) $dE/dt^{(1/2)}$ curves from b), e) and h) of LIBs the ball milled Cu+2Ge+3P samples.

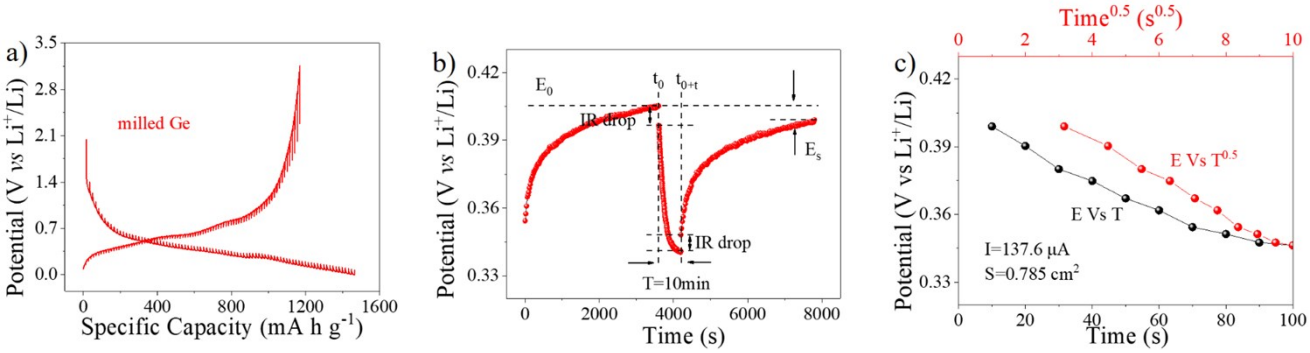

Fig. S18. a) Galvanostatic intermittent titration technique (GITT) profiles during pristine discharge and charge of LIBs utilizing milled Ge as electrodes; b) the typical schemes for single-step of GITT experiments of LIBs utilizing milled Ge as electrodes; c) $dE/dt^{(1/2)}$ curves from b) of LIBs utilizing milled Ge as electrodes.

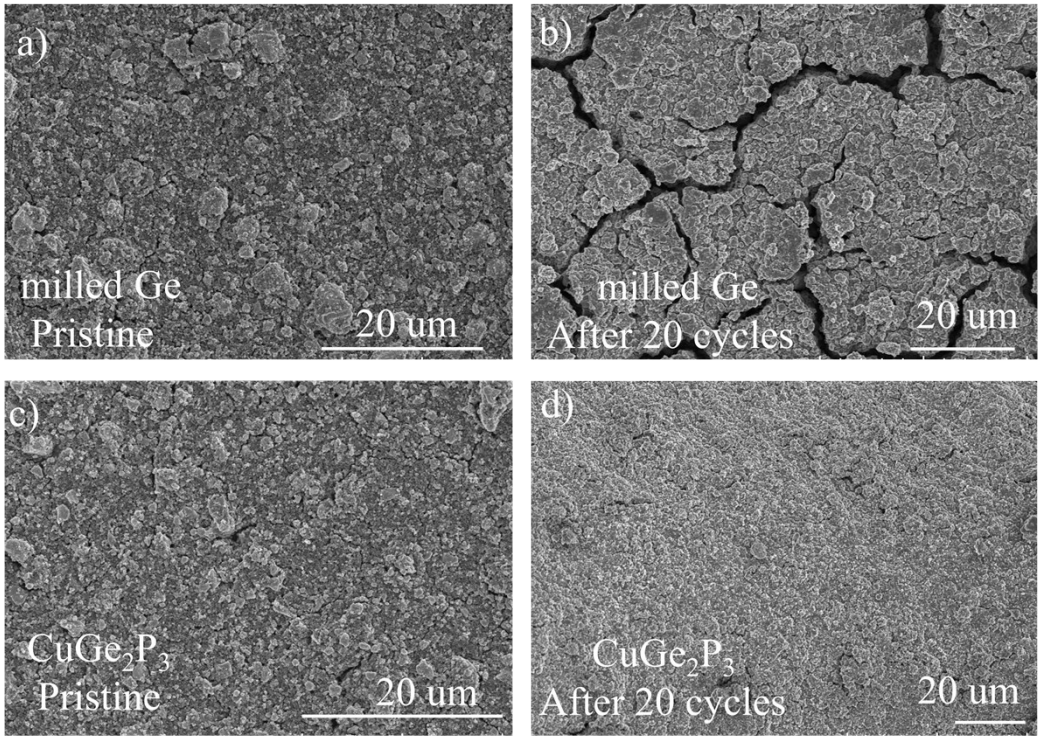

Fig. S19. SEM images of the cation-disordered $CuGe_2P_3$ compound and milled Ge electrodes: a) milled Ge electrodes before cycling, b) milled Ge electrodes after 20 cycles at 100 mA g^{-1}, c) cation-disordered $CuGe_2P_3$ compound electrodes before cycling, d) the cation-disordered $CuGe_2P_3$ compound electrodes after 20 cycles at 100 mA g^{-1}.

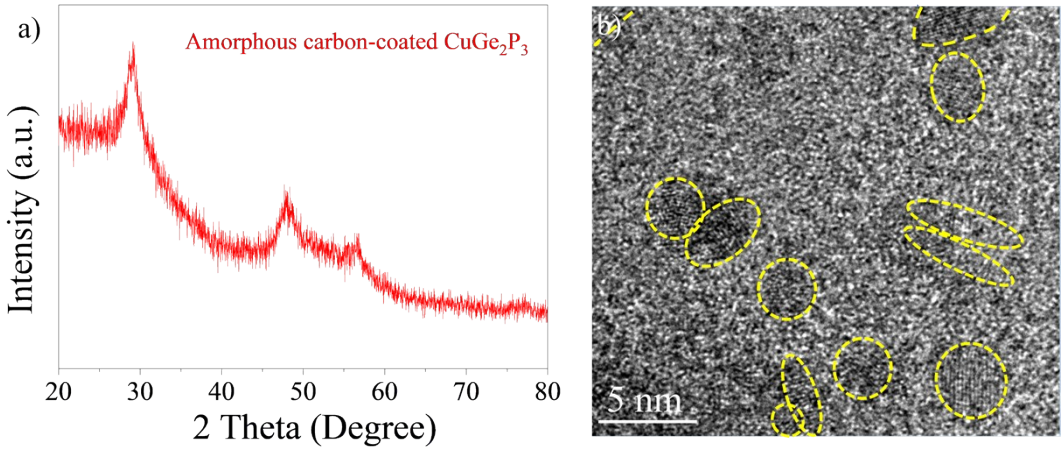

Fig. S20. a) XRD pattern and b) HRTEM image of the amorphous carbon-coated the cation-disordered $CuGe_2P_3$ compound. The broadened XRD diffraction peaks and the low intensity, along with the disappearance of graphite indicate that the particle size of the as-synthesized $CuGe_2P_3$ was significantly decreased and embedded into the amorphous carbon.

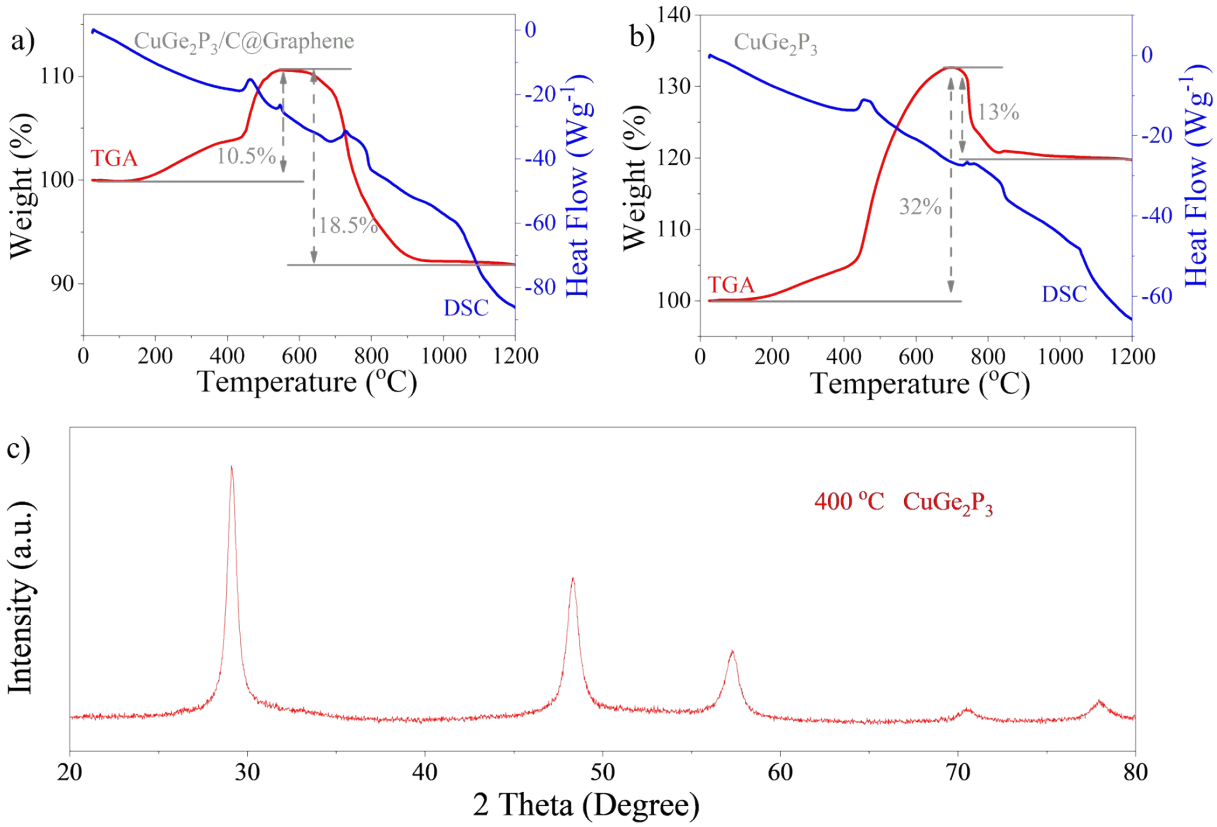

Fig. S21. a-b) TGA curves of $CuGe_2P_3$/C@Graphene and b) the $CuGe_2P_3$ compound; c) XRD pattern of $CuGe_2P_3$ under 400°C in air for 3h.

Note that the carbon content is calculated as follows:

Carbon content in the composite is x and $CuGe_2P_3$ is y.

x + y =1 (Equation 1);

1.19y = 0.92 (Equation 2).

According to the above equations, the carbon content (x) can be obtained to be 22.69 %, which is close to the feed ratio of the two components.

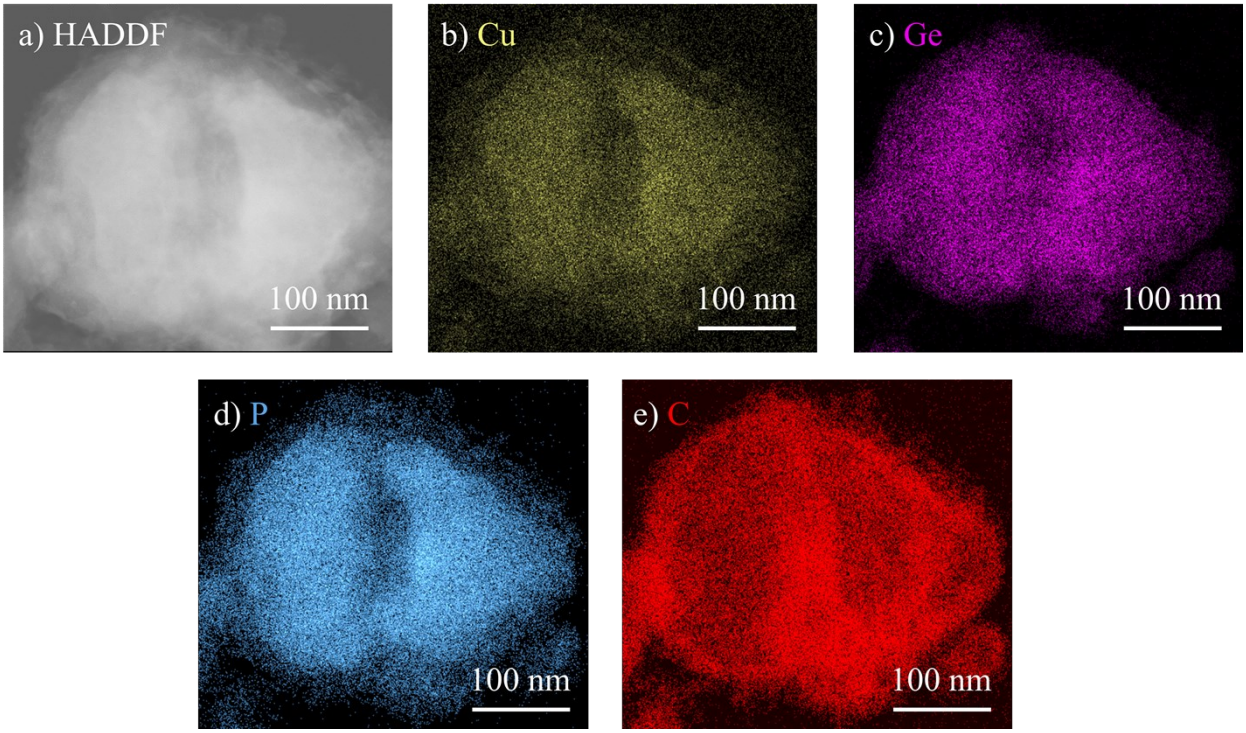

Fig. S22. Low magnification TEM image and elemental mappings of $CuGe_2P_3$/C@Graphene.

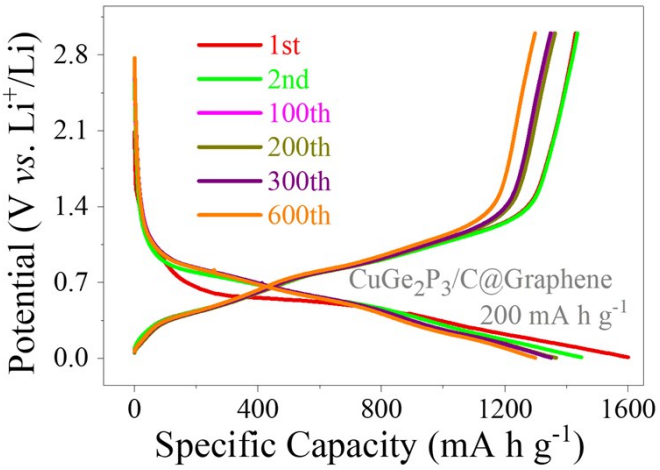

Fig. S23. Voltage profiles of different cycling conditions of $CuGe_2P_3$/C@Graphene at 200 mA h g^{-1}.

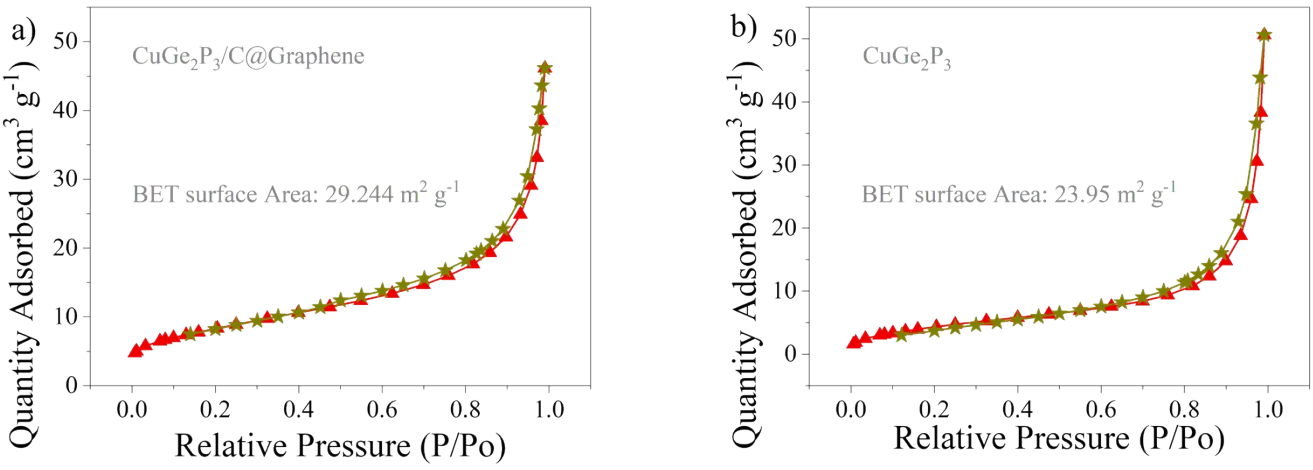

Fig. S24. BET curves of a) $CuGe_2P_3$/C@Graphene and b) Cation-disordered $CuGe_2P_3$ compound.

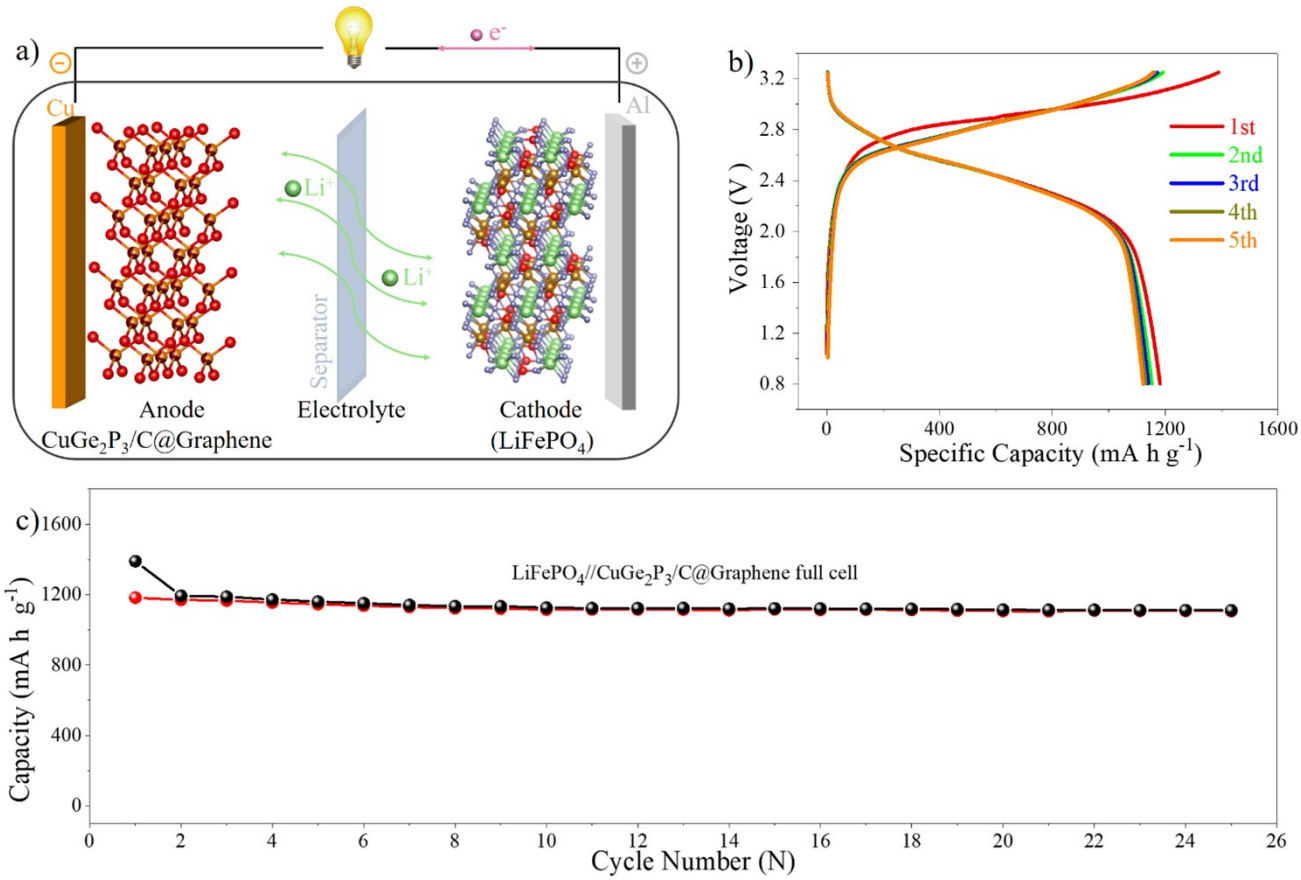

Fig. S25. The $LiFePO_4$//$CuGe_2P_3$/C@Graphene full cell: a) a schematic sketch of the full cell; b) the first five discharge-charge profiles; c) cycle performance.

Table S5. Performances comparisons of $CuGe_2P_3$/C@Graphene with recently reported Ge-based anodes in terms of initial Coulombic efficiency and long cycling stability.

Materials	Cycle performance	Initial Coulombic efficiency	References
$CuGe_2P_3$/C@Graphene	0.02 A g^{-1}, 600 cycles, 1312 mA h g^{-1}	91%	This work
Li_2GeO_3	0.05 A g^{-1}, 300 cycles, 725 mA h g^{-1}	56%	[49]
$Ge_{0.90}Ga_{0.10}$	0.32 A g^{-1}, 150 cycles, 1146 mA h g^{-1}	85%	[50]
GeP_3/C	0.1 A g^{-1}, 130 cycles, 1109 mA h g^{-1}	73.8%	[51]
GeSn	0.2 C, 25 cycles, 1040 mA h g^{-1}	83%	[52]
$Ge_{0.85}Te_{0.15}$	1 C, 500 cycles, 1002 mA h g^{-1}	70.4%	[53]
GeS	0.16 A g^{-1}, 100 cycles, 1150 mA h g^{-1}	78%	[54]
3D-pGe	1.147 A g^{-1}, 250 cycles, 770 mA h g^{-1}	92.3%	[55]
Si-Ge hNWs	1 C, 400 cycles, 300 mA h g^{-1}	74.7%	[56]
Ge_3N_4@C	0.69 A g^{-1}, 300 cycles, 660 mA h g^{-1}	78%	[57]
NPGeNFs	3 C, 500 cycles, 678 mA h g^{-1}	81.8%	[58]
$Ge_2Sb_2Se_5$	0.5 C, 100 cycles, 626 mA h g^{-1}	68%	[59]
Ge-HS/GNs	0.8 A g^{-1}, 500 cycles, 1182 mA h g^{-1}	83.6%	[60]
rGO/Ge/rGO	1.6 A g^{-1}, 500 cycles, 1085 mA h g^{-1}	69.6%	[61]
Ge (ZnRR)	0.08 A g^{-1}, 300 cycles, 1030 mA h g^{-1}	81%	[62]
Li_2TiGeO_5	1 A g^{-1}, 600 cycles, 406 mA h g^{-1}	68%	[63]
Ge@MoS_2	7 A g^{-1}, 100 cycles, 594 mA h g^{-1}	79.6%	[64]
Ge-S-C	0.1 A g^{-1}, 100 cycles, 1114 mA h g^{-1}	77.7%	[65]
Fe-GeO_2	1 A g^{-1}, 100 cycles, 1114 mA h g^{-1}	58.76%	[66]

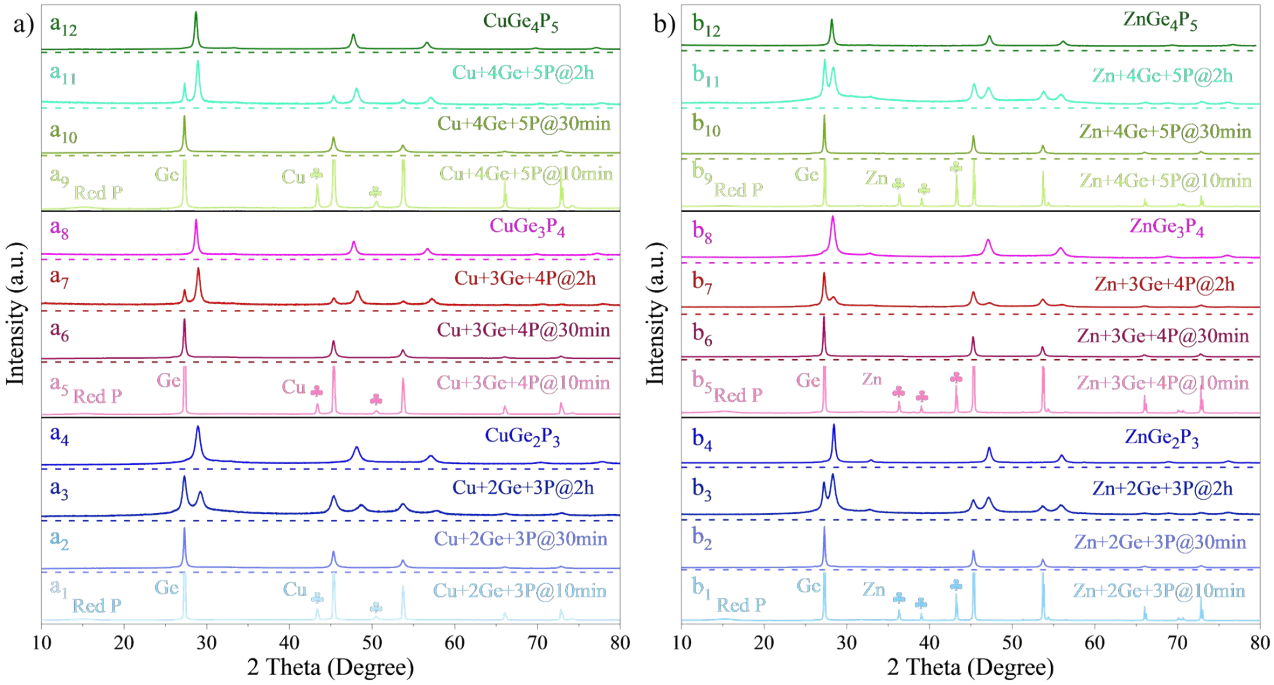

Fig. S26. Evolved XRD patterns of the Cu(Zn)-Ge-P samples of Cu(Zn)+2Ge+3P, Cu(Zn)+3Ge+4P, and Cu(Zn)+4Ge+5P samples.

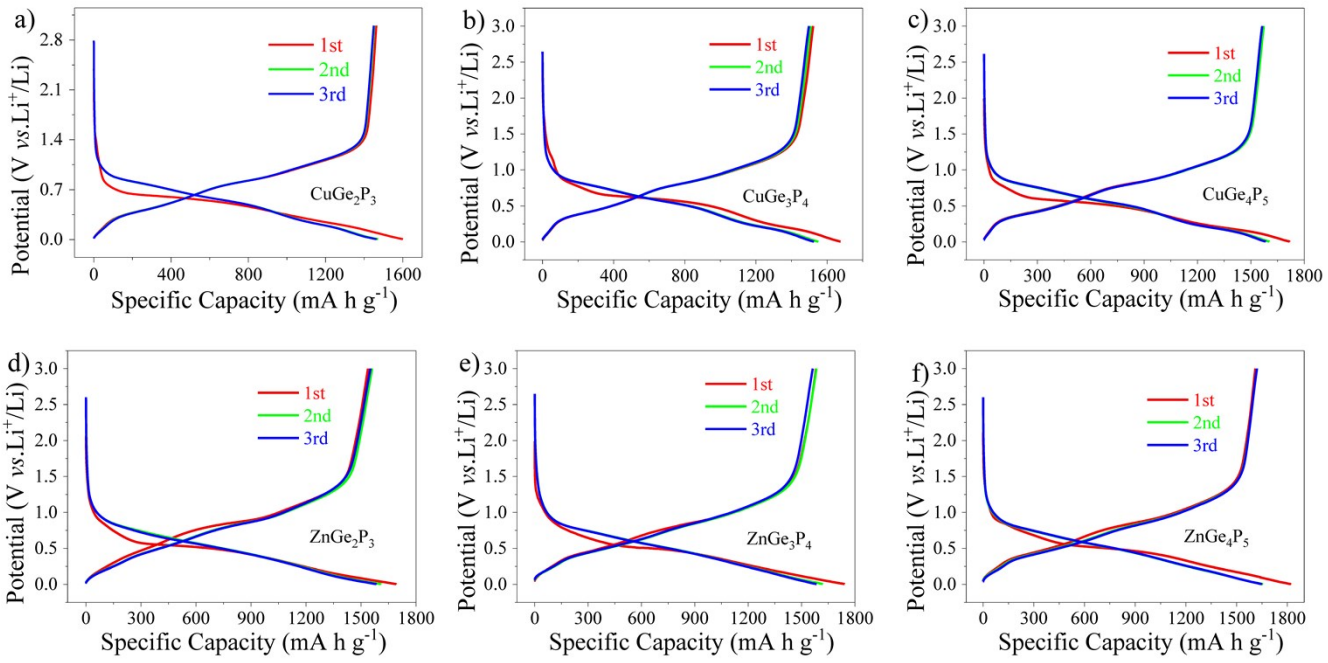

Fig. S27. Initial three discharge-charge curves of the cation-disordered Cu(Zn)-Ge-P compounds ($Cu(Zn)Ge_2P_3$ → $Cu(Zn)Ge_3P_4$ → $Cu(Zn)Ge_4P_5$.

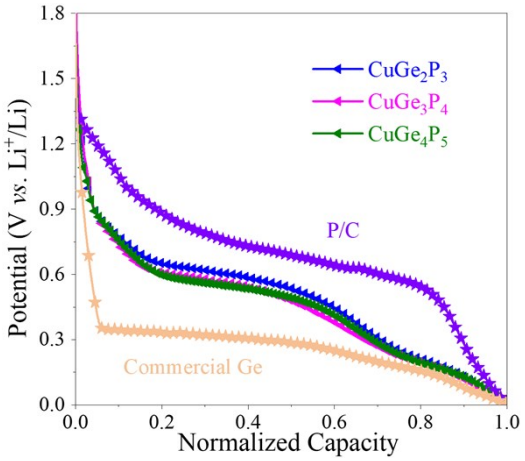

Fig. S28. Typical discharge profiles of the cation-disordered Cu-Ge-P compounds ($CuGe_2P_3$ → $CuGe_3P_4$ → $CuGe_4P_5$), commercial Ge and P/C electrodes.